Impedance measures for a better understanding of the electrical stimulation of the inner ear

Quentin Mesnildrey, Frédéric Venail, Robert P Carlyon, Olivier Macherey

Making corrections to your proof Please follow these instructions to mark changes or add notes to your proof. You can use Adobe Acrobat Reader

Olivier Macherey

IOP Publishing Journal of Neural Engineering
J. Neural Eng. **00** (2018) 000000 (18pp) UNCORRECTED PROOF

Impedance measures for a better understanding of the electrical stimulation of the inner ear

AQ1

Quentin Mesnildrey[1,3], Olivier Macherey[1], Philippe Herzog[1] and Frédéric Venail[2]

[1] Aix Marseille Univ., CNRS, Centrale Marseille, LMA, Marseille, France
[2] ENT Department and Montpellier University, Gui de Chauliac University Hospital

AQ2

AQ3 E-mail: xxxx

Received 7 May 2018, revised 6 October 2018
Accepted for publication 31 October 2018
Published

Abstract

AQ4 The performance of cochlear implant (CI) listeners is limited by several factors among which the lack of spatial selectivity of the electrical stimulation. Recently, many studies have explored the use of multipolar strategies where several electrodes are stimulated simultaneously to focus the electrical field in a restricted region of the cochlea. These strategies are based on several assumptions concerning the electrical properties of the inner ear that need validation. The first, often implicit, assumption is that the medium is purely resistive and that the current waveforms produced by several electrodes sum linearly. In experiment 1, several impedance measurements were carried out *in vitro* and in eight CI users using sinusoidal and pulsatile waveforms to test this hypothesis. High-resolution voltage recordings (1.1 MHz sampling) were obtained and showed the resistivity assumption to be valid at 46.4 kHz, the highest frequency tested. However, these measures also revealed the presence of parasitic capacitive effects arising from the device at high frequency that could be deleterious to these strategies.

Multipolar strategies also require an estimation of the contribution of each electrode to the overall electrical field. This can be partly obtained by measuring the impedance matrix. However, measuring the voltage on active electrodes (i.e. the diagonal of the matrix) is not straightforward because of the polarization of the electrode-fluid interface. Existing multipolar strategies use linear extrapolation from measurements made at neighboring electrodes to infer this value. In experiment 2, we use a simple model including a constant phase element in order to isolate the polarization component of the contact impedance. We show that this model can fit the high-resolution impedance measurements better than previous approaches in the CI field that used resistor-capacitance circuit models despite using the same number of variables. Implications for the design of multipolar strategies are discussed.

Keywords: current focusing, cochlear implant, impedance measure, electrical field imaging

AQ5 (Some figures may appear in colour only in the online journal)

1. Introduction

AQ6

In normal hearing, the cochlea behaves as a frequency analyzer and initiates neural activity in different auditory nerve fibers depending on the frequency content of the incoming sound. In deaf patients implanted with a cochlear implant (CI), spectro-temporal sound features are delivered by a dozen electrodes implanted in one of the fluid-filled chambers of the cochlea called the scala tympani (ST). The different electrodes target different subpopulations of auditory nerve fibers and are also stimulated according to the frequency content of the sound in order to mimic the excitation produced in a normal ear.

[3] Author to whom any correspondence should be addressed.

JNL:JNE PIPS: AAECFF TYPE: PAP TS: NEWGEN DATE:9/11/18 EDITOR: IOP SPELLING: UK

Even though many studies reported good speech recognition abilities in silence, most CI users perform poorly in noisy environments (Friesen *et al* 2001), and have difficulties to discriminate between speakers or to appreciate music (McDermott 2004). A commonly-acknowledged reason for this poor performance is the lack of spatial selectivity of the electrical stimulation. Contemporary CIs use monopolar stimulation (MP), where electrical current flows from a stimulating electrode and widely spreads across the conductive perilymph of the ST. It then leaves the cochlea to reach the ground electrode located in the temporal muscle. Each electrode thus presumably stimulates a large portion of the cochlea. Activating several electrodes yields interferences which distort the pattern of neural activity produced along the cochlea and deteriorate the transmission of sound information.

Several alternative multi-electrode stimulation modes have been designed to improve the spatial selectivity of electrical stimuli and thus reduce those interactions but the benefits of these focused stimulation strategies for speech recognition by CI listeners have shown mixed results (reviewed in Mesnildrey and Macherey (2015)). To efficiently control the electrical spread using multi-electrode stimulation, it appears necessary to better understand the electrical behavior of the human inner ear.

For a given patient, the electrical field produced by the activation of an electrode can be measured on other inactive electrodes (Vanpoucke *et al* 2004a, van den Honert and Kelsall 2007). The recorded voltage can then be normalized by the amplitude of the current input and expressed in terms of electrical impedance. In the present study, *transimpedance* measurements refer to voltage recordings made between an inactive intracochlear electrode and the remote ground when another intracochlear electrode is activated with reference to the same ground. Measuring transimpedances between all stimulating-recording electrode combinations, yields the so-called impedance matrix. By inverting this matrix, it is theoretically possible to infer the currents to apply to all electrodes simultaneously to produce an arbitrary voltage vector along the electrode array. Using estimations or measurements of the current spread for the design of highly-focused stimulation strategies has been introduced in early CI studies (von Compernolle 1985, Townshend and White 1987). More recently, van den Honert and Kelsall (2007) have proposed a practical implementation of such a strategy known as the phased array (PA) strategy. Computational modeling studies of the human cochlea (Frijns *et al* 2011, Kalkman *et al* 2015) suggested that PA stimulation should also reduce the spread of excitation at the level of the auditory nerve compared to MP. However, as pointed out by Kalkman *et al* (2015) this ability to produce narrow excitation patterns may depend on several factors such as the electrode-to-neurons distance and the state of neural degeneration. While a benefit in spatial selectivity of PA was demonstrated electrophysiologically at the level of the inferior colliculus of deafened cats (George *et al* 2014), results in human studies are less clear. Smith *et al* (2013) demonstrated better performance of CI listeners in a spectral ripple discrimination task for PA compared to MP suggesting a benefit in spatial selectivity. However, using a different (forward masking) paradigm, Marozeau *et al* (2015) did not find any differences between the widths of the neural excitation patterns produced by MP and PA.

These somewhat inconsistent results may have various causes, including the use of different implementations of the PA strategy. Here, we evaluate two hypotheses on which the PA strategy is based, in order to better understand the properties of the intracochlear medium and propose alternatives for its implementation.

The most fundamental assumption implicitly used in this strategy, as well as in other multipolar strategies such as tripolar, is that, despite the presence of different biological materials in the inner ear, the overall medium can be considered as purely resistive. This implies that stimulating an electrode with a biphasic current pulse instantly produces in the cochlea a biphasic voltage pulse whose amplitude results from the resistance of the current pathway. Another consequence of this resistivity assumption is that the contributions of different electrodes add linearly within the cochlea. In experiment 1, several measurements were carried out, both *in vitro* and in CI users, to verify the validity of these assumptions.

A second assumption relates to voltage measurements made between active electrodes and the ground to estimate the diagonal terms of the impedance matrix. When an electrode is activated, the passage of current from the electrode to the perilymph requires a transition between electrical charge carriers and ionic charge carriers. This transition consists in an important charge reorganization at the electrode-fluid interface known as the charge double layer (Gouy 1910, Grahame 1947, Dymond 1976). The ionic current then flows through cochlear tissues and fluids to reach the ground electrode. Voltage is measured between the active contact and the ground electrode whose area is assumed to be large enough so that it is not polarizable. The recorded waveforms are distorted by the polarized interface of the intracochlear electrode which prevents a straightforward estimation of the resistive path between the electrode surface and the ground (*i.e. the access resistance*). van den Honert and Kelsall (2007) proposed an estimation of the diagonal terms using linear extrapolation from transimpedance measurements on adjacent electrodes. However, since the impedance matrix is inverted to determine what current level to send on each electrode, a poor estimation of the diagonal terms could strongly deteriorate current focusing. In experiment 2, electrode polarization was studied *in vitro* and in CI users. A simple electrical model was used to estimate the contact impedance and to infer the tissue impedance. A proper estimation of the tissue impedance would provide a fully-determined impedance matrix and might open new perspectives for further improvements of focused electrical stimulation.

2. General methods

2.1. Device specifications

In vitro and *in vivo* experiments were carried out using the HiRes 90k Device (Advanced Bionics ®) connected to the HiFocus 1J electrode array which consists of 16 rectangular

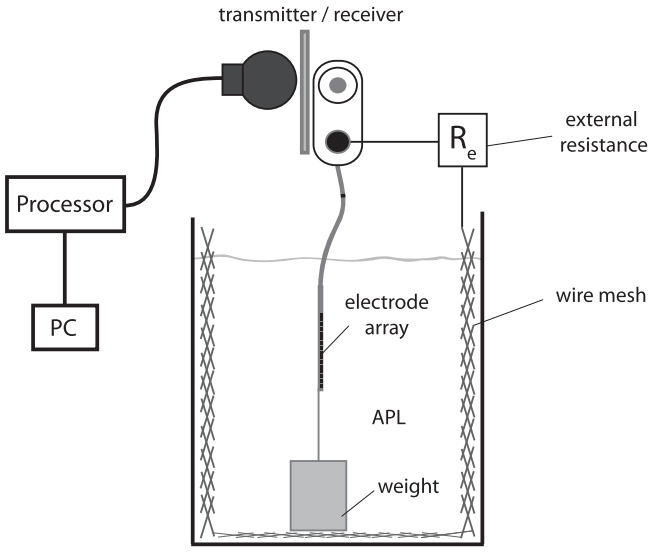

Figure 1. Experimental *in vitro* setup.

(0.5×0.4 mm^2 surface) platinum contacts spaced by 1.1 mm and recessed in a silicon carrier. Stimulation and measurements were made using custom software implemented in Matlab (The MathWorks, Natick, MA, 2010) which served as an interface to the BEDCS software (Bionic Ear Data Collection System, Advanced Bionics ®, (Litvak 2003)).

2.2. In vitro setup

An *in vitro* experimental setup (figure 1) was designed so that the HiFocus 1J electrode array was immersed in artificial perilymph (APL). APL was initially made following Desmadryl *et al* (2012) yielding a resistivity of 80 $\Omega \cdot$ cm. However, Baumann *et al* (1997) pointed out that the conductivity of human cerebrospinal fluid increases by approximately 23% between room temperature and body temperature. The present ionic solution as well as the commonly used value of 70 $\Omega \cdot$ cm (Finley *et al* 1990, Strelioff 1973, Suesserman and Spelman 1993) thus probably overestimate the resistivity of the real inner ear perilymph at body temperature, supposedly around 55 $\Omega \cdot$ cm (Baumann *et al* 1997). To carry these experiments at room temperature (≈20 °C) while considering more realistic values of conductivity, NaCl was added to the original APL to match the conductivity of the actual perilymph at body temperature.

The electrode array was maintained vertically with a small weight attached to the apical end of the silicon carrier while the receiver and the ground electrode remained outside the solution. The tank sides were covered with a stainless steel wire mesh connected to the ground with an external resistor R_e to mimic the resistive path between the inner ear and the temporal muscle.

This setup provides a controlled environment that approximates free field stimulation in a homogeneous medium. The possibility to vary R_e enables investigating its influence independently from the other parameters and also provides impedance measures with orders of magnitude closer to those measured with CI users.

Table 1. CI subjects details (S1–S8) with duration of deafness, etiology, duration of implant use, and age.

Subject	Duration of deafness prior to CI (years)	Etiology	CI use (years)	Age
S1	20	Unknown progressive	12	38
S2	7	Unknown progressive	7	62
S3	1	Unknown progressive	11	76
S4	21	Unknown progressive	13	52
S5	Unknown	Genetic	7	48
S6	6	Usher syndrome	13	20
S7	24	Pendred syndrome	12	39
S8	2	Unknown progressive	15	87

2.3. CI users

8 adult CI users took part in this experiment and were paid for their participation. All subjects were implanted with the HiFocus 1J electrode array. Subjects' details are reported in table 1. It is important to note, as we will see later in this article, that none of these participants had deactivated electrodes at the moment of the experiment and that all electrodes were used daily, in normal conditions. Experiments carried out with CI users were approved by the local ethics committee (Eudract 2012-A00438-35).

2.4. Stimuli

Stimuli were electrical pulses or sinusoids presented either in monopolar mode with reference to the case electrode, or in bipolar mode.

Electrical pulses were symmetric and biphasic (anodic-first, unless otherwise stated) and had no interphase gap. Their phase duration ranged from 17.96 μs to 99 μs and they were presented at a current level ranging from 25 μA to 100 μA.

One period of a sinusoid was created by concatenating either 24 or 36 monophasic pulses, the duration of these pulses was adjusted between 0.898 and 208 μs depending on the frequency of the sinusoid. Fifteen different sinusoids with frequencies logarithmically spaced in the (0.2–46.4) kHz range were tested. Several periods of each sinusoid could be obtained by repeating this pattern. The memory capacity of the present device is shared between the stimulating stage and the recording stage. The actual buffer duration is thus dependent on both the sampling rate, and the complexity of the stimulus (i.e. the number of monophasic segments used to define it). As a result, the total duration of the sinusoidal stimuli was chosen depending on the available space in the device buffer and varied between 0.15 ms and 33.33 ms (see details in table 2).

In CI users, detection thresholds for sinusoidal stimuli drop dramatically when the frequency decreases below 300

Table 2. Details on sinusoidal stimuli.

Frequency (kHz)	Pulses per period	Phase duration (μs)	Number of periods	Stimuli duration (ms)
0.20	24	208	6	29.95
0.30	24	141	10	33.33
0.43	24	96.1	10	23.26
0.64	36	43.1	10	15.63
0.94	36	29.6	12	12.77
1.41	36	19.8	20	14.18
2.12	24	19.8	30	14.15
3.09	24	8.98	35	11.33
4.42	36	6.29	40	9.05
6.63	24	6.29	55	8.30
10.31[a]	36	2.69	5	0.49
15.47[a]	24	2.69	7	0.45
23.20[a]	24	1.80	7	0.31
30.93[a]	36	0.898	5	0.16
46.40[a]	24	0.898	7	0.15

[a] Recordings made using the up-sampling procedure (see section 2.5).

Hz (Pfingst 1988). To avoid exposing subjects to loud stimuli, we measured the most comfortable levels (MCLs) for several 200 Hz stimuli on all tested electrodes. The stimulation level used for the experiment (for all electrodes) was then equal to the minimum MCL across electrodes.

Most of the stimuli used in this series of recordings were subthreshold or just audible. Relatively low levels were chosen to ensure patients' comfort during the session.

2.5. Recording

The BEDCS software (Litvak 2003) enables recording the electrical voltage across a given pair of electrodes. Here, recordings were made between one intracochlear electrode and the large ground electrode, unless otherwise stated. Voltage waveforms were then normalized by the input current level to be expressed in Ohms. The present device is provided with an adaptable amplifier gain (1 dB–1000 dB) and sampling rate (ranging from 9 kHz to 55.6 kHz). However, for the scope of the present study, a higher resolution was sometimes required to record fast onset and offset transients for biphasic pulses and also high frequency sinusoids (higher than 9 kHz) with a resolution of at least 15 samples per period. To achieve a higher sampling rate, the following upsampling technique was used. With a 55.6 kHz sampling rate, samples are taken every 17.96 μs synchronized with the internal clock. To be able to measure the voltage waveform within the inter-sample time of 17.96 μs, several additional recordings were made by introducing small known delays. The different recordings were then concatenated offline. Given the minimal time step of 0.898 μs, the maximum sampling rate is 1.1 MHz. Additional control recordings were carried out with and without the upsampling procedure to make sure that the phase and magnitude of the recorded waveforms were identical in both cases. This provided an indirect check for this upsampling method. For biphasic pulses, the waveforms were analyzed in the time domain while for sinusoids, amplitude and phase were obtained by fitting (nonlinear least-square fitting) delayed sine waves with a frequency equal to the input frequency (table 2). Note that for frequencies ranging from 0.64 kHz to 6.63 kHz, a small DC component was removed using the *detrend* function in Matlab. Magnitude and phase were plotted and analyzed using Bode diagrams. Specific stimulation or recording parameters are further described for each experiment.

3. Experiment 1: Resistivity and linearity

3.1. Resistivity

3.1.1. Rationale and methods. Multipolar stimulation strategies rely on the assumption that the inner ear is purely resistive. In other words, it is assumed that a constant current source creates inside the cochlea an instantaneous voltage deviation proportional to the current level. Several early animal studies demonstrated the validity of this assumption up to 12.5 kHz (e.g. Clopton and Spelman (1982) and Suesserman and Spelman (1993)). Vanpoucke *et al* (2004b) also validated this assumption in human CI recipients but only up to 12 kHz. Besides, their analysis was restricted to magnitude changes and did not consider a possible frequency dependence of the phase. Since contemporary CIs use biphasic pulses with very steep transients, the spectrum of these electrical signals contains components at frequencies higher than 12 kHz. It is, therefore, important to know if the resistivity hypothesis still holds at higher frequencies.

Herein, impedance spectroscopy measures were carried out both *in vitro* and in human CI subjects in the (0.2–46.4) kHz frequency range to investigate a possible frequency dependence of transimpedance magnitude and phase. For each electrode, the transimpedance on an adjacent electrode was also measured for biphasic pulses to evaluate the consistency of the recorded electrical waveforms and assess the presence of any potential distortion.

In CI users, three stimulating electrodes, located at the apical, medial and basal part of the array were used: electrodes 1, 8 and 16. Electrode 1 was first used as the stimulating

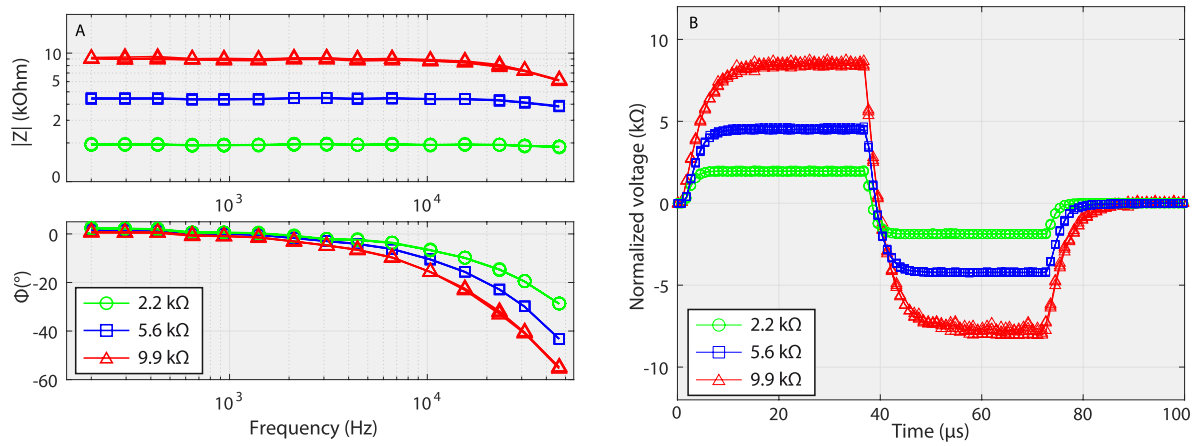

Figure 2. Panel (A) Bode diagram from transimpedance spectroscopy measured *in vitro* for various values of R_e. For each R_e, measurements were made for stimulating-recording pairs 1–2, 4–5, 8–9, 12–13, 16–15. Panel (B) Impedance waveforms measured *in vitro* for biphasic pulse inputs using different values of R_e. For each R_e, measurements were made for stimulating-recording pairs 1–2, 4–5, 8–9, 12–13, 16–15 and yielded similar outputs.

electrode while recording electrodes were separated by either one, five, ten or fifteen electrodes (i.e. electrodes 2, 6, 11, 16), resulting in a minimum and maximum spacing of 1.1 mm and 16.5 mm, respectively. Similar recordings were made using electrode 16 as the stimulating electrode and recording on electrodes 15, 11, 6, and 1. Finally electrode 8 was used as the stimulating electrode and electrodes 1, 4, 7, 9, 12, 16 as recording electrodes. We hypothesized that the presence of capacitive components along the current pathway (i.e. perilymph, bones or tissues) would be associated with an influence of the inter-electrode distance on the phase and magnitude impedance spectra. To evaluate the level dependence of spectroscopy data, additional measurements were carried out at a lower current level for a subset of electrode pairs (1–2, 8–9, and 16–15) and at three frequencies (0.64, 2.12, and 10.31 kHz).

3.1.2. Preliminary in vitro experiment: parasitic capacitance. To define a baseline for the analysis of CI data, transimpedance spectroscopy was first carried out *in vitro* for different values of R_e (2.2, 5.6 and 9.9 kΩ). For each R_e, stimulation was made on electrode 1, 4, 8, 12, and 16 the and voltage was recorded on an adjacent electrode (i.e. electrodes 2, 5, 9, 13, and 15 respectively) with reference to the ground.

Figure 2(A) displays the Bode diagram for all 15 conditions. Different electrode conditions yielded identical patterns. One can note a slight decrease of magnitude above 30 kHz associated with a more visible phase shift. Increasing R_e amplifies this effect which is inconsistent with a purely resistive behavior and thus suggests the presence of capacitive components *within* the circuit comprising device electronics, platinum-iridium wires, electrodes and the APL.

Figure 2(B) shows the transimpedance waveforms measured with biphasic pulses in the same 15 conditions. The low-pass filtering mentioned above resulted in smooth exponential transients at the onsets, offsets and phase reversals.

Even though the capacitive behavior of the APL is theoretically negligible (Schwan and Calvin 1957), additional measures (data not shown here) were carried out to identify the source of these capacitive components. The transmitter was first connected to an experimental load board where current sources output can be displayed on an oscilloscope (i.e. without APL). Using the experimental setup shown in figure 1, voltage was also measured across R_e using a differential probe (Hameg Instruments®, HZ109).

In this configuration, both spectroscopy data and biphasic pulses exhibited a comparable low-pass filtering which suggests that this effect is only dependent on the resistive load and not on the electrolyte per se. This capacitive behavior can thus be fully attributed to a parasitic capacitance, C_p, emerging from current sources imperfections and the proximity between individual wires and the device electronics (Barbour 2014, Scholvin *et al* 2016). To estimate the order of magnitude of C_p, the entire transimpedance matrix was measured *in vitro* using the up-sampling procedure for $R_e = 5.6$ kΩ. All waveforms were normalized and the exponential transients' time constants were estimated. This yielded a very consistent estimation of 0.38 nF (s.d. = 0.004 nF).

3.1.3. Evaluating the resistivity assumption in CIs. Even though the ionic composition of the APL is supposedly close to that of the human perilymph, the human inner ear is composed of different media which may not all be resistive. With CI subjects, the resistance between a given electrode and the ground (referred to as the access resistance) is unknown but supposedly constant and recordings can only be made using intracochlear electrodes. In this configuration, a potential capacitive behavior of the cochlear fluids and tissues would be mixed with C_p and thus difficult to identify. The presence of capacitive materials was investigated by varying the distance between the stimulating and the recording electrodes. Figure 3(A) shows a typical Bode diagram measured in one CI subject (S3) for stimulating-recording electrodes pairs 1–2, 1–6, 1–11, and 1–16.

For all subjects, varying the stimulation level did not affect spectroscopy data (Red + symbols in figure 3(A)). In the high frequency range (>10 kHz), all spectroscopy data showed a phase shift comparable to that observed *in vitro*. To separate

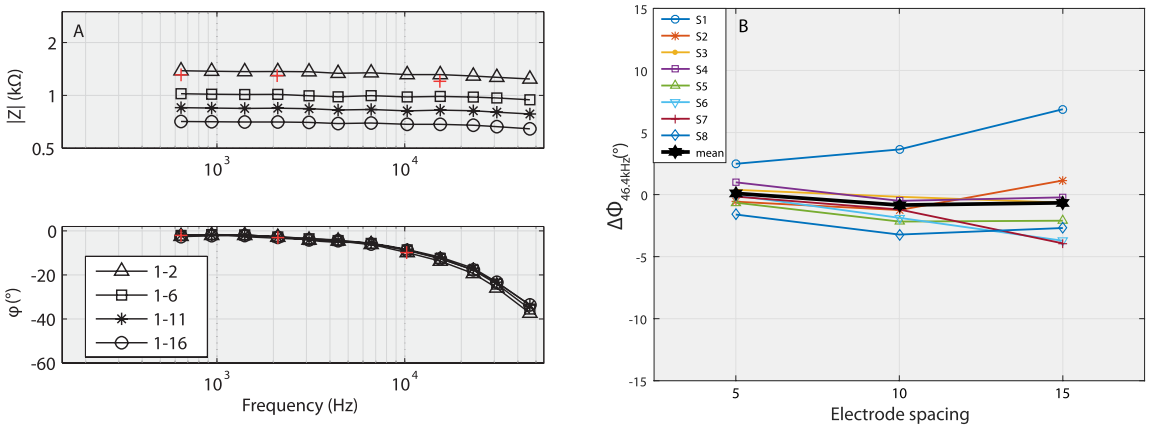

Figure 3. Panel (A) Bode diagram from transimpedance spectroscopy measured in subject S3 with an amplitude of 25 μA. Electrode 1 was used as the stimulating electrode and recordings were made on electrode 2, 6, 11, and 16. The red + symbols represent the additional data recorded using electrodes 1–2 with an amplitude of 10 μA. Panel (B) Phase angle in degrees at 46.4 kHz relative to its value for a spacing of one electrode as a function of electrode spacing (expressed in number of electrodes). Each symbol is for one CI subject with electrode 1 as the stimulating electrode. The thick black curve indicates the mean $\Delta\phi$.

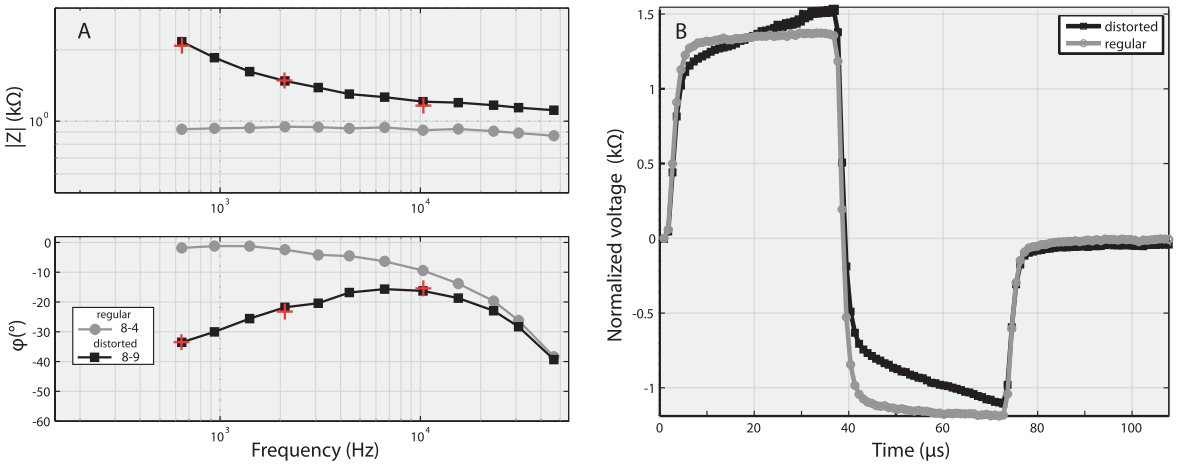

Figure 4. Panel (A) Bode diagram from transimpedance spectroscopy with 10 μA stimuli measured in S5. Regular data (grey circles) were recorded using stimulating-recording electrodes 8–4 and distorted data (black squares) were recording using electrodes 8–9. Red + symbols represent additional data recorded using electrodes 8–9, with an amplitude of 5 μA . Panel (B) Up-sampled transimpedance waveforms for 50 μA biphasic pulse input measured in S5. Regular data (grey circles) were recorded using stimulating-recording electrodes 1–2 and distorted data (black squares) were recording using electrodes 8–9.

the contribution of C_p from a possible capacitive behavior of biological media, the effect of longer current path on phase shift was examined by plotting $\Delta\phi_{46.4\text{ kHz}}$, defined as the variation of the phase angle at 46.4 kHz as a function of electrode spacing relative to that obtained for a spacing of one electrode. Figure 3(B) illustrates the variation of $\Delta\phi_{46.4\text{ kHz}}$ when electrode 1 was used as stimulating electrode for all subjects. In this representation, we hypothesize that an additional capacitive effect introduced by long current pathways would yield a monotonic decrease of $\Delta\phi_{46.4\text{ kHz}}$ as a function of the inter-electrode distance. Herein, no such trend was observed and the maximal value for $\Delta\phi_{46.4\text{ kHz}}$ remained lower than an error of one sample (similar observations were made when using electrodes 16 of 8 as stimulating electrodes). This suggests that the high frequency phase shift is independent of the electrode separation and that it is thus associated with C_p only. The effect of C_p is only effective at high frequency, thereby distorting biphasic current pulses at onsets, offsets and phase reversals. The voltage response can, therefore, be described by a biphasic voltage pulse with exponential transients.

Among the 112 transimpedance spectroscopy measurements carried out in CIs during this experiment (14 conditions × 8 subjects), 23 recordings in four subjects (S5, S6, S7 and S8) not only exhibited a high-frequency phase shift due to the presence of C_p but also an unexpected *low-frequency phase shift* associated with an increase in amplitude. Figure 4(A) compares regular and distorted spectroscopy data measured with subject S5 for different electrode pairs. This suggests a capacitive charging of the inactive recording electrodes.

A comparable distortion could also be observed in the time domain when measuring transimpedance waveforms with biphasic pulses as illustrated in figure 4(B).

To quantify the conditions where distorted signals occurred, we analyzed the entire transimpedance matrix measured with 50 μA biphasic pulse and 100 μs phase duration using the maximum sampling rate of the present device

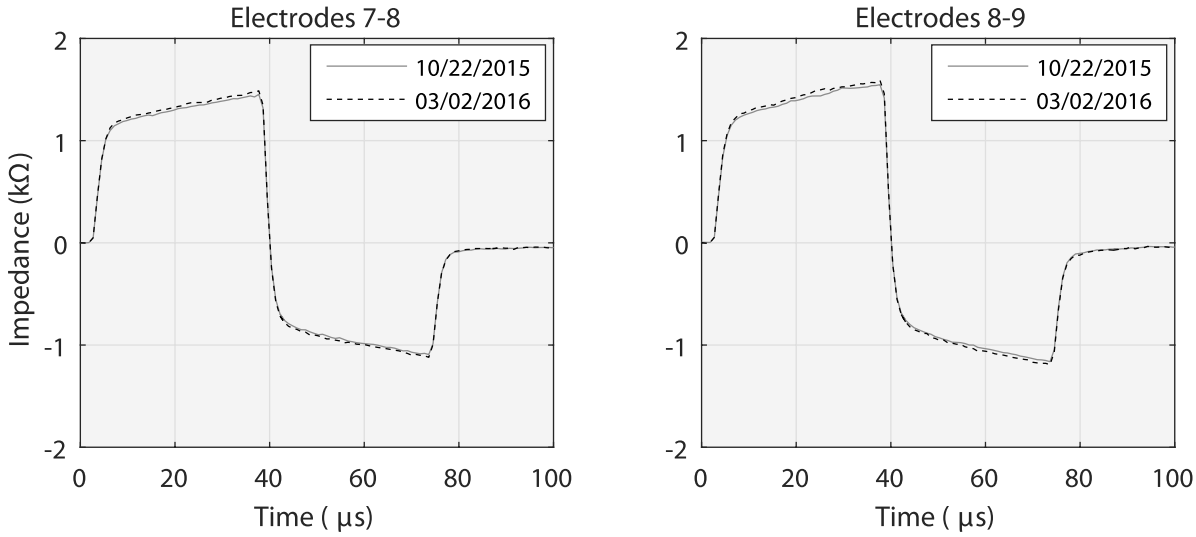

Figure 5. Two examples of upsampled transimpedance recordings measured with S5 during the initial session (grey curves) and five months later (black dashed curves).

(55.6 kHz). Impedance waveforms were normalized and fitted with a biphasic pulse with exponential transients. When analyzing the sum of square errors (SSE), we noticed that SSEs exhibited a bimodal distribution with a narrow peak between 0 and 0.015 (centered at 0.004) and a second shallower peak for SSEs larger than 0.015 (centered at 0.028). Hence, we arbitrarily defined waveforms showing a sum of squared error higher than 0.015 as distorted. As a result, 18% of the 1920 (16×15 electrode combinations $\times$ 8 subjects) waveforms could be reported as distorted.

To better understand this phenomenon, it is also worth noting that, first, this distortion is associated with specific pairs of stimulating-recording electrodes and not to individual electrode's interface. In other words, it could occur when stimulating electrode X and recording on electrode Y (and reciprocally) but not necessarily when stimulating electrode X and recording on electrode Z or when stimulating electrode Z and recording on electrode Y. Second, additional recordings were carried out with S4 and S5 in the same configuration respectively one month and five months after the initial session. In both cases, neither the amplitude nor the shape of the distortion were affected by this delay, demonstrating good repeatability and stability over time (figure 5). Possible explanations for this phenomenon are discussed in section 5.

3.2. Linearity

3.2.1. Rationale and method. In the PA strategy, the spatially-selective electrical pattern results from the linear sum of the electrical fields produced by each individual electrode. To efficiently control channel interactions, it is thus necessary to ensure that no distortion is induced by electrical field summation. Series of measurements were carried out to investigate the linearity of current summation *in vitro* and in CI users. Those measurements consisted in activating a pair of electrodes with biphasic pulses of the same amplitude (50 μA) but opposite polarities, and measuring the voltage between one inactive electrode located in between the stimulating electrodes and the ground. For each subject, different electrode pairs were chosen in the apical, middle and basal sections of the array. All recordings were up-sampled[4]. The amplitude of the recorded waveform was then compared to the value inferred from the linear sum of transimpedance measurements made in MP mode.

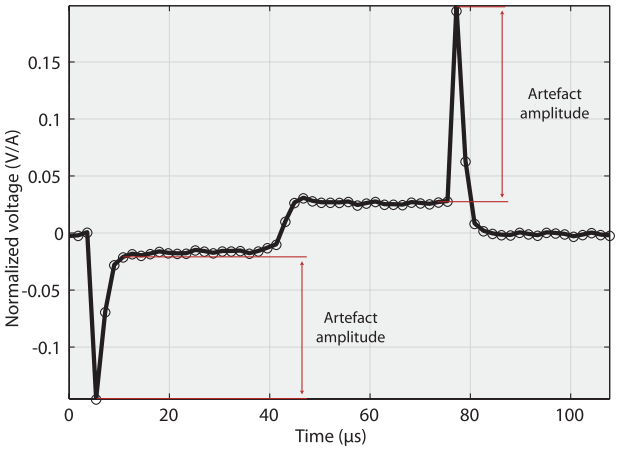

Figure 6. Current summation from the bipolar stimulation of electrodes 7 and 9 measured on electrode 8, in subject S2.

3.2.2. Results. Figure 6 shows a typical resulting waveform measured in subject S2. Assessing the linearity of current summation was not straightforward not only because of the peaky artifacts located at the onset and offset, but also because some waveforms were affected by the same distortion as in section 3.1.

The amplitude of the recorded waveforms was thus arbitrarily defined as half the difference between the amplitude of the first phase (measured three samples after the peak of the onset artifact) and the amplitude of the second phase

[4] The combination of BP stimulation and a full up-sampling up to 1.1 MHz exceeds the performance of the device. To run these measurements, the sampling rate was reduced to 557 kHz.

(measured six samples after the peak of the phase reversal artifact). This estimation was then compared to the theoretical amplitude inferred from the transimpedance matrix. Overall the amplitude of the electrical field superimposition could be predicted from transimpedance data with an average error of 31Ω (s.d. = 30Ω). This result validates the assumption of linearity for current summation. Besides, for five subjects who participated in this experiment, we also measured one column of the impedance matrix at 25 μA and 100 μA to evaluate the variation of the transimpedances with the stimulation level. These recordings showed that across this (small) range of levels, transimpedance values varied by less than 5%.

The artifacts at onset and offset can be explained by an imperfect superimposition of individual electrical fields due to transient time constants discrepancies. These differences in time constants arise from the different values of the resistive paths between each electrode and the ground coupled to the parasitic capacitance. Similar patterns were obtained in all subjects and also *in vitro* even with time constant differences smaller than 0.2 μs. The amplitude of the onset and offset artifacts was measured relative to the following or preceding phase respectively (i.e. relative to the expected amplitude). For all recordings carried out in CIs the mean amplitude was estimated at 192Ω (s.d. = 84Ω). Since those artifacts arise from simultaneous interactions, their amplitude will increase with the amplitude of the original stimuli. Here, recordings were made at a very low level (50 μA) and none of the eight participants reported an auditory percept. It is however complicated to predict if such artifacts might become audible at higher levels. Consequences of these artifacts as well as possible solutions to reduce them are discussed later in section 5.

4. Experiment 2: Contact impedance

4.1. Rationale and methods

4.1.1. Rationale. As previously mentioned, the contact impedance is defined as the voltage difference between an active electrode and the ground electrode divided by the injected current amplitude. It thus theoretically provides information on the path between one stimulating electrode and the ground. Unfortunately, the polarization of the electrode-fluid interface distorts the recorded waveforms and prevents a straightforward estimation of the access resistance. A modeling approach, as described in the next paragraph is thus often necessary.

In the field of neural prostheses (e.g. CI or retina implants), being able to estimate the access resistance is a crucial challenge for several reasons. First, it can be used as a clinical follow-up to make sure all electrodes are functioning normally. Second, some studies investigated the possibility to use impedance measures to obtain some information on the surrounding biological medium (Newbold *et al* 2004) or the electrode placement (Pham *et al* 2013, Majdi *et al* 2015).

4.1.2. Equivalent electrical circuit. The commonly-used approach to model electrode polarization is by means of equivalent electrical circuits. In human CI recipients, some studies have proposed a simple description of this phenomenon including the resistance of the current path from the electrode to the ground in series with the polarization impedance composed of a capacitance in parallel with a charge transfer resistance (Newbold *et al* 2004, Vanpoucke *et al* 2004a, Tykocinski *et al* 2005).

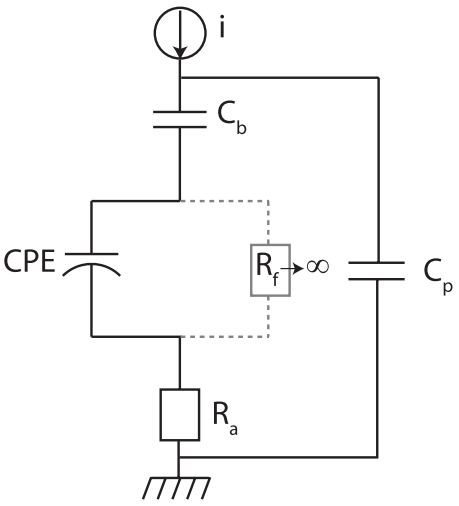

Figure 7. Electrical model of the electrode-electrolyte interface.

However, several *in vitro* and animal studies provided a good account of this phenomenon using more advanced equivalent electrical circuits and recording systems (e.g. Duan *et al* (2004) and Franks *et al* (2005)). Herein we used a simple phenomenological model derived from those studies to describe contact impedance. This model (figure 7) consists of five components including a known blocking capacitor, C_b ($C_b = 100$ nF), a constant phase element, CPE (equation (1)), modeling the behavior of the charge double-layer at the electrolyte interface, a Faradaic resistance, R_f, associated with the transition from electrical to ionic charge carriers, the access resistance, R_a, modeling the overall resistance of current pathways, and the parasitic capacitance, C_p introduced in section 3.1.

The access resistance may result from several contributions: a parasitic resistance due to the device (switches, wires, amplifier, etc R_d), and the spreading resistance ($R_{spreading}$) representing the current pathway from the electrode to the ground. The spreading resistance for a rectangular electrode (one-side exposed) can be estimated using equation (2), where ρ is the resistivity of the medium in $\Omega \cdot$ cm, l and w represent the length and with of the electrode (Kovacs 1994, Franks *et al* 2005).

$$Z_{CPE} = \frac{1}{Y_0 \cdot (j\omega)^{\alpha}} \tag{1}$$

$$R_{spreading} = \rho \cdot \frac{\ln(4 \cdot l/w)}{\pi \cdot l}. \tag{2}$$

The equivalent circuit impedance equation was converted to the Laplace domain to determine the analytical solution in the time domain considering biphasic current pulses (see appendix, (Lario-García and Pallàs-Areny 2006)). Model parameters (R_a, R_f, Y_0, α, C_p) were estimated by fitting

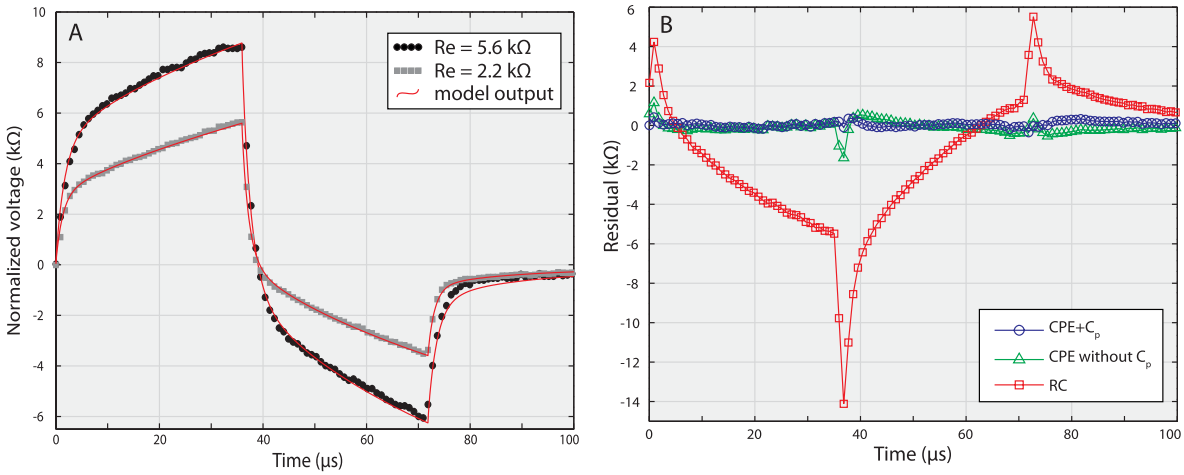

Figure 8. Panel (A) Contact impedance waveforms recorded *in vitro* for $R_e = 2.2$ kΩ (grey squares) and 5.6 kΩ (black dots) and model outputs. Panel (B) Residual of different contact impedance model fittings: a resistor-capacitor (RC) model similar to what is commonly used to fit CI impedance data ((Newbold *et al* 2004, Vanpoucke *et al* 2004a, Tykocinski *et al* 2005), squares), the model with a CPE presented in figure 7 with (circles) and without C_p (triangles).

(nonlinear least-squares method) normalized potential waveforms with this analytical solution. Unlike models used in human CI studies (Vanpoucke *et al* 2004a, Tykocinski *et al* 2005), the capacitive element of the polarized interface was modeled by estimating both the amplitude and the α coefficient.

Spectroscopy data were also used to estimate model parameters using EIS spectrum analyzer software (Bondarenko and Ragoisha 2005) and the Nelder–Mead simplex algorithm (Nelder and Mead 1965).

4.1.3. Measurements. In CIs, all contact impedances were measured using the up-sampling procedure for 50 μA biphasic pulses with a 35.92 μs phase duration. This condition is referred to as the *default condition* in the following paragraphs. Additional measures were obtained on a subset of electrodes (Electrodes 1, 4, 8, 12, and 16) to evaluate the robustness of the parameters' estimation. This included varying the level (25 and 100 μA) or the phase duration (17.96 μs and 67.35 μs), or the leading polarity of the pulses. Contact impedance spectroscopy was also measured for all contacts on the entire frequency range ([0.2–46.4] kHz). For CI listeners, the amplitude of sinusoids was chosen depending on the comfortable level obtained at 200 Hz determined in experiment 1. Electrode polarization strongly increases the peak amplitude of impedance recordings. A relatively low level was thus used in order to record all contact impedances at the same level and prevent the saturation of the internal amplifier. The possible influence of the stimulation level is further discussed in section 5.2.

4.2. Results: in vitro data

The present electrical model shown in figure 7, as well as the classic RC model (Vanpoucke *et al* 2004a, Tykocinski *et al* 2005), were first fitted to the *in vitro* data. *In vitro* measurements yielded a very high estimation for R_f ($>10^{15}\Omega$) which means that the kinetics of the dissolution of the platinum

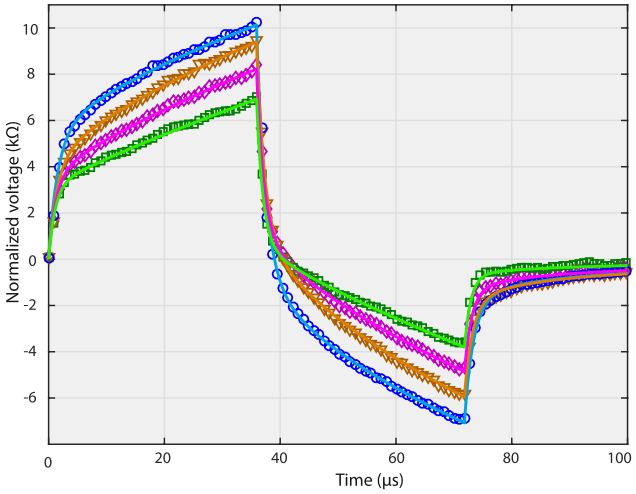

Figure 9. Four examples of contact impedance waveforms (each symbol is for one electrode) and model output (Solid lines) measured with S2 in the *default condition* (50 μA biphasic pulses with a 35.92 μs phase duration).

electrode into the electrolyte is extremely slow (Wieckowski 1999). In the following, therefore, this phenomenon was neglected. R_f was removed from the equivalent circuit and another analytical solution was computed to fit the data. Note this did not affect the estimation of the other parameters.

Figure 8(A) represents the impedance waveforms and the present model output for $R_e = 2.2$ kΩ and $R_e = 5.6$ kΩ. For each case, the estimation of the access resistance was 2.85 kΩ, and 6.18 kΩ respectively. In the present experimental conditions, $R_{spreading}$ should be approximately equal to 565Ω, implying that the contribution of R_d is probably small (85 Ω and 15 Ω respectively).

Figure 8(B) displays the residual of three different models: RC, CPE with and without C_p, applied on the same data as in figure 8(A), for $R_e = 2.2$ kΩ. Those preliminary measurements show that, first, a CPE is more appropriate to model the polarization impedance, and second, including C_p is

Table 3. Model parameters for all CI subjects estimated from anodic-first biphasic pulses with a 50 μA amplitude and a 35.92 μs phase duration.

	R_a (kΩ)		$Y_0(\Omega^{-1} \cdot j\omega^{\alpha}) \cdot 10^{-9}$		α		C_p (nF)	
	Mean	Range	Mean	Range	Mean	Range	Mean	Range
S1	5.76	[4.73–7.29]	712	[319–1010]	0.58	[0.53–0.67]	0.23	[0.20–0.25]
S2	3.20	[2.40–4.55]	427	[95–770]	0.64	[0.56–0.78]	0.39	[0.32–0.46]
S3	3.62	[2.46–5.06]	533	[74–928]	0.64	[0.56–0.83]	0.35	[0.24–0.45]
S4	4.54	[3.30–6.37]	558	[223–891]	0.62	[0.54–0.71]	0.28	[0.23–0.32]
S5	3.55	[1.63–6.93]	258	[91–601]	0.66	[0.54–0.77]	0.44	[0.30–0.60]
S6	3.35	[2.53–4.79]	245	[46–564]	0.73	[0.60–0.87]	0.39	[0.31–0.47]
S7	4.63	[3.12–5.56]	672	[354–1119]	0.59	[0.55–0.64]	0.29	[0.23–0.37]
S8	4.14	[2.15–6.42]	442	[86–891]	0.64	[0.54–0.81]	0.36	[0.26–0.60]
Average	4.01		481		0.64		0.34	

absolutely necessary for the fitting of the entire impedance waveform and especially for the estimation of R_a. It is worth noting that, if R_f is removed from our model, the number of parameters to fit is identical to the classical RC model used in previous CI studies (Vanpoucke *et al* 2004a, Tykocinski *et al* 2005) but yields a much better fit.

4.3. Results: CI users data

Contact impedances were measured for all available electrodes and all CI users. All waveforms could be described by the present model ($r^2 > 0.98$ for all electrodes).

Figure 9 shows an example of contact impedance waveforms for four different electrodes measured in subject S2 (symbols figure 9) and the corresponding model outputs (solid lines).

The overall dataset for CI users yielded very subject-specific across-electrode patterns for R_a. Table 3 gives a summary of the averaged fitted parameter values as well as the minimum and maximum values across the array for each subjects in the default condition.

The robustness of the model was investigated by varying the amplitude, phase duration, and leading polarity of the pulses for a subset of electrodes, resulting in five estimations of the model parameters obtained from independent measurements. For each subject, each electrode within this subset, and each parameter, the coefficient of variation (CV) across the five conditions was calculated[5]. Figure 10(A) displays the individual CVs expressed in percentage. Each data point relates to one of the electrodes measured in a given subject and different symbols are for different subjects. Averaged across subjects and electrodes, the mean CV was: 7.3% for R_a, 33.2% for Y_0, 7.7% for α, and 18.2% for C_p.

The model parameters were also estimated from impedance spectroscopy data for all electrodes. Figure 10(B) represents the individual estimation of model parameters obtained in the spectral domain versus those obtained in the time domain. Here again, each data point relates to one electrode and different symbols are for different subjects. Data points located above the diagonal indicate a higher estimation using spectroscopy data than using biphasic pulses. Overall, one can note that the values of R_a and C_p remain very consistent across all conditions in both the spectral and temporal domain while Y_0 and α exhibited much more variation across the different conditions.

In figure 10(B), it is worth noting that the range of Y_0 was smaller using the spectroscopy data than the biphasic pulse data, except for one subject who showed surprisingly high values for Y_0 associated with very low α. Possible explanations for the variability of the estimation observed between different stimuli will be discussed in section 5.2.

5. Discussion

5.1. Experiment 1

5.1.1. Parasitic capacitance, C_p. In experiment 1, impedance spectroscopy enabled us to assess the presence of a parasitic capacitance, C_p, which resulted in a low-pass filtering of the stimulus waveform. To our knowledge, in previous *in vitro*, *in vivo* or model CI studies, pulsatile stimuli were always considered as perfect square pulses. Franks *et al* (2005) pointed out a comparable phase drop at high frequency ($f > 100$ kHz) in their *in vitro* spectroscopy data but they argued that this was more likely due to the measurement system. *In vitro*, the influence of C_p on electrical stimuli might not be an issue when the access resistance is very low, for instance when the ground is located in the saline solution, which seems to be the case for a number of studies (Ifukube and White 1987, Suesserman *et al* 1991, Franks *et al* 2005, Tognola *et al* 2007). In this situation, its effect would be constrained to the very high frequency domain. However, the present results suggest that C_p must not be neglected when using this device in CIs and it is likely that other devices also show a similar behavior.

We have seen in the present study that the presence of C_p yields some smoothing of the biphasic pulses transients. With this simple model representation, the time constant of the circuit is given by the product of R_a and C_p. As a result, because of the across-electrode variations of the access resistance (and potentially additional small variations of C_p), each source generates current pulses with slightly different transients. When different electrical fields are superimposed, this mismatch

[5] The CV was defined as the standard deviation divided by the mean except for α which is distributed on a bounded scale. For this parameter CV was defined according to Burdon (2008).

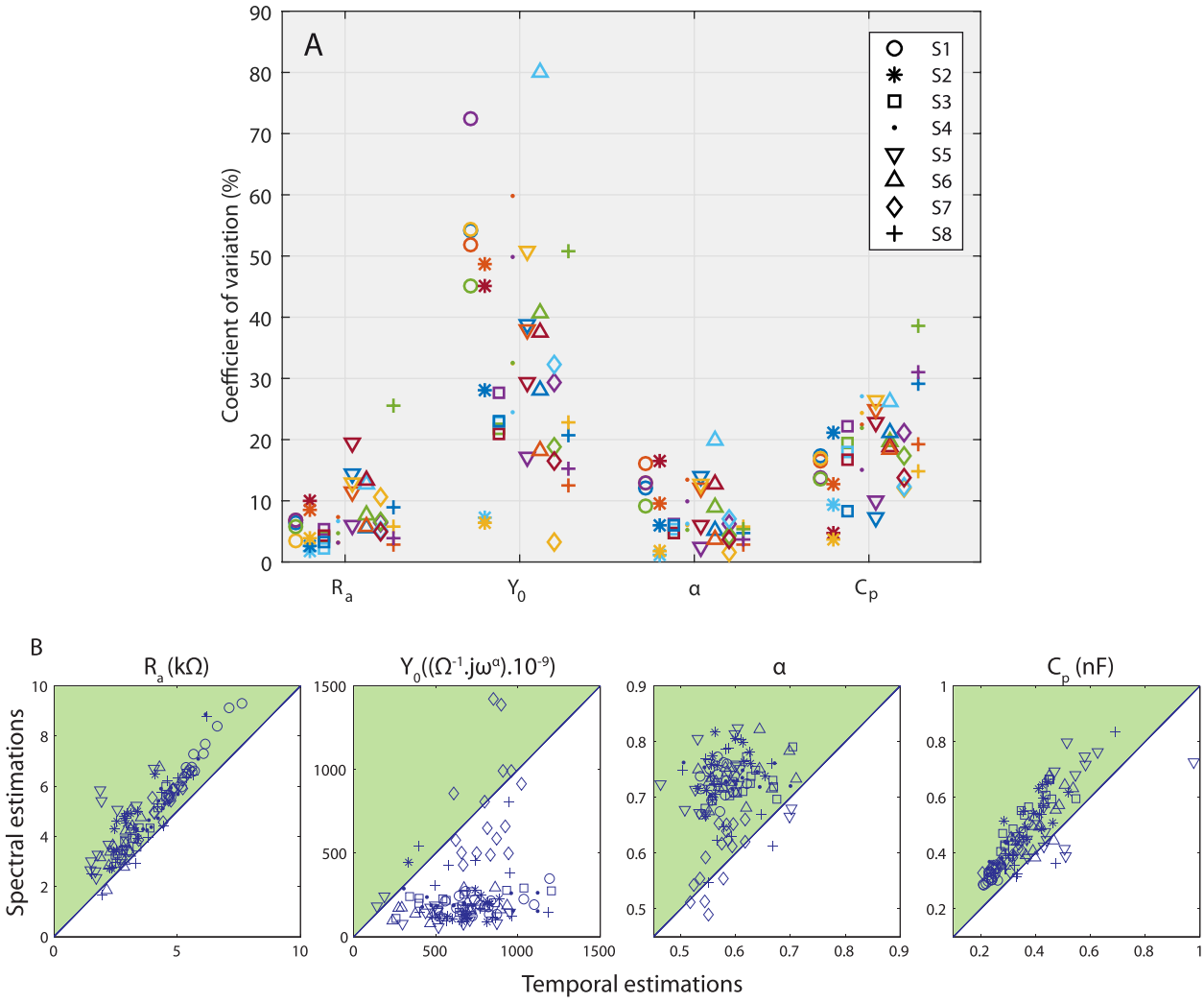

Figure 10. Panel (A) Coefficient of variation of model parameters estimates using different stimuli. Panel (B) Spectral domain estimation versus time domain estimation of model parameters. From left to right: R_a, Y_0, α, C_p. Each data point corresponds to one electrode for one subject, different symbols are for different subjects.

yields voltage transient artifacts as shown in figure 6. As a consequence, such artifacts are expected to occur in other multipolar stimulation modes (e.g. tripolar). It might be especially problematic for the PA strategy since the residual electrical field would present unwanted voltage peaks. As these artifacts result from an imperfect cancellation of two (or several) pulses, their amplitude is proportional to the amplitude of the original stimuli. We may thus expect high-amplitude artifacts to occur in the vicinity of the stimulating electrode. To better control the electrical field produced in the cochlea by a CI, it might be beneficial to consider using single-cycle sinusoids or Gaussian-shaped pulses as alternative pulse shapes to restrain the spectral content of the stimulus waveform to lower frequencies. Recordings similar to those carried out in section 3.2 were done in CIs, using single-cycle sine waves. Figure 11 shows typical waveforms recorded in subject S8 on electrodes 2 resulting from the bipolar stimulation of electrodes 1–3. One can note that the summation artifacts located at the onset, offset and phase reversal (solid line) are much smaller when using single-cycle sine waves (dashed line).

As mentioned earlier, these artifacts could only be observed using upsampled recordings, and we would not expect them to last for more than a few microseconds. To address the question of the possible influence of these artifacts at the perceptual level, one has to consider the strength-duration function of a typical auditory nerve fiber, and the fact that the neural membrane would act as a leaky integrator of charge (Abbas and Miller 2006). Several studies measured the strength-duration function in CI users (Moon *et al* 1993, Miller *et al* 1999, Chatterjee and Kulkarni 2014). They reported a consistent decrease in threshold of approximately 5 dB per doubling of the phase duration. We may thus expect a pulsatile stimulus made of 3 μs long artifacts to have a detection threshold several dozens of decibels higher than a stimulus with a standard phase duration at the same stimulation rate. However, to our knowledge none of these studies investigated the evolution of detection thresholds for phase durations below 10 μs. Therefore, without further investigation, it remains unclear whether these artefacts may produce neural responses on their own.

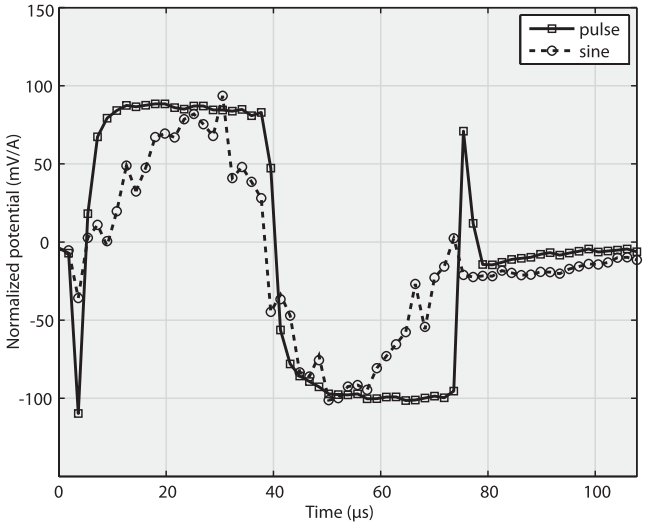

Figure 11. Normalized potential resulting from current summation using biphasic pulses (solid line) and single cycle sine waves (dashed line) measured in subject S8. Electrode pair 1–3 was stimulated in bipolar mode and voltage was recorded on electrode 2.

5.1.2. Resistivity and partial polarization. While the present measurements enabled the verification of the resistive behavior of the inner ear at high frequency, it also revealed the presence of a non-resistive phenomenon at low frequencies. Since these distorted waveforms showed close similarities with the contact impedance waveforms, it is possible that this behavior results from the partial polarization of inactive electrodes. This partial polarization might be explained by the combination of several factors.

Non-resistive biological materials. It is first possible that current lines pass through biological materials that are not purely resistive over this frequency range. Grill and Mortimer (1994) reported that a layer of macrophages, foreign body giant cells, loose collagen, and fibroblasts could form around epoxy electrode arrays. They observed that the electrical impedance of this layer showed a frequency-dependency suggesting a capacitive behavior. However, the effect was limited to very low frequencies (<100 Hz) and was not obtained with silicon carriers. Furthermore, a closer view at our transimpedance recordings seems to contradict this explanation. If one considers electrode 2 as the stimulating electrode, one might expect the voltage recorded on electrodes 14, 15 and 16 to reflect the influence of comparable current pathways. However, in the case of S8, in this specific configuration electrodes 14 and 16 yielded distorted patterns but not electrode 15.

Charge deposition on the recording electrode. It is possible that this partial polarization arises because of a charge deposition on the recording electrodes. This might first occur within the device, if the proximity of wires within the silicon carrier creates a stray capacitance and that few electrical charges deposit on the metallic surface of the recording electrodes (Fridman and Karunasiri 2010). Charge deposition might also occur in the cochlear medium because of a deviation of current lines towards the electrodes when passing in the very vicinity of the highly conductive platinum surface (Grimnes and Martinsen 2008). Even though the use of recessed contacts supposedly limits this phenomenon, it might be facilitated if the electrodes are constrained in fibrous tissues or even bone due to a traumatic insertion or a specific deafness etiology. Consequently, current stimuli delivered by one of those electrodes would be forced to pass along other inactive electrodes.

Electrode surface modifications. Finally, the presence of this distortion seemed at least partially related to the patients' fitting history and especially the way the device was (or was not) used.

For S7, all electrode pairs yielded distorted waveforms. Interestingly, it happens that this patient had troubles to adapt to her implant and initially only relied on residual hearing from her contralateral ear. Therefore, she had barely used her implant for about eight years before reactivating it after the loss of her residual hearing.

For S8, measurements involving even electrodes yielded distorted signals and we suspect that this patient used, years ago, an early strategy where every other electrode was turned off[6]. Figure 12 represents the normalized transimpedance recorded in S8. Panel (A) displays the recordings obtained with all odd stimulating electrodes, panel (B) displays the recordings obtained with even stimulating electrodes and odd recording electrodes and panel (C) displays the recordings obtained with even stimulating electrodes and even recording electrodes. We can note that no distortion at all is observed with odd stimulating electrodes, while almost all waveforms are distorted when both the stimulating and recording electrodes are even electrodes.

We know from contact impedance studies that the electrical properties of the electrode-fluid interface are modified when an electrode is left unstimulated (Newbold *et al* 2004, Wilk *et al* 2016).

First, the coupling between the electrode and the cochlear medium might be modified due to the presence of resistive fibrous tissues on its surface. In particular Duan *et al* (2004) pointed out that for frequencies below 100 kHz, ionic current is directly dependent on the amount of extracellular fluid. A poor coupling due to the deficiency of perilymph, or the presence of inflammatory cells or tissues on the electrode may impact ionic conduction in the vicinity of the electrode. Second, the reaction between the perilymph and the metallic surface might create an oxidation layer, known as the passivation layer (López *et al* 2008). After a relatively short period of time, electrical stimulation of the electrodes is supposed to (1) disrupt the cell layer (Newbold *et al* 2004), and (2) induce a partial removal of the passivation layer (Topalov *et al* 2014). Here, in both cases, an abnormally long period of inactivity might have permanently altered the electrodes' electrochemical properties.

[6] Unfortunately we did not have access to this patient clinical file to confirm our speculations. The original Advanced Bionics electrode array had eight medial facing contacts and eight lateral facing contacts (Stickney *et al* 2006). When the CII implant was launched (in summer 2000 in Europe), while featured with sixteen medial facing electrodes, the original numbering of a subset of eight (even or odd) electrodes was initially used to be compatible with former implants and strategies (Brendel *et al* 2013). Engineers from Advanced Bionics acknowledged an increase in the impedance of inactive electrodes with patients fitted with a similar electrode configuration.

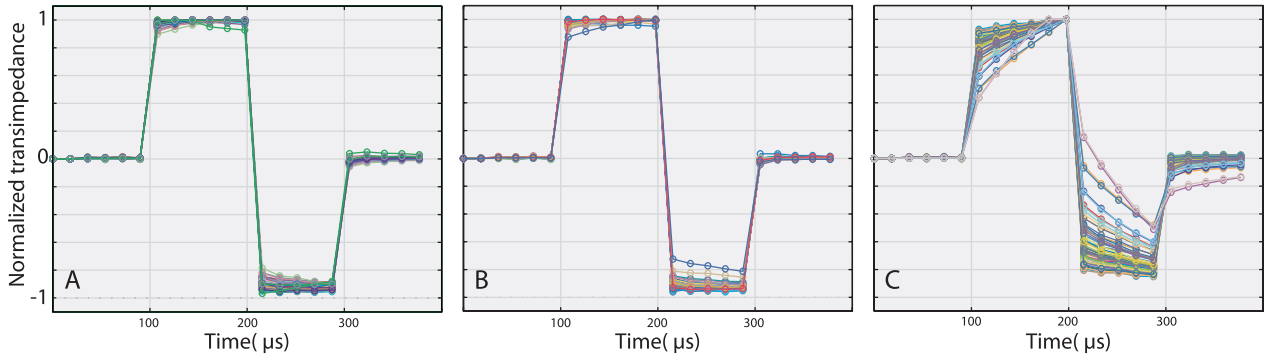

Figure 12. Normalized transimpedance recording made with S8. Panel (A) displays the recordings obtained with all odd stimulating electrodes, panel (B) displays the recordings obtained with even stimulating electrodes and odd recording electrodes and panel (C) displays the recordings obtained with even stimulating electrodes and even recording electrodes.

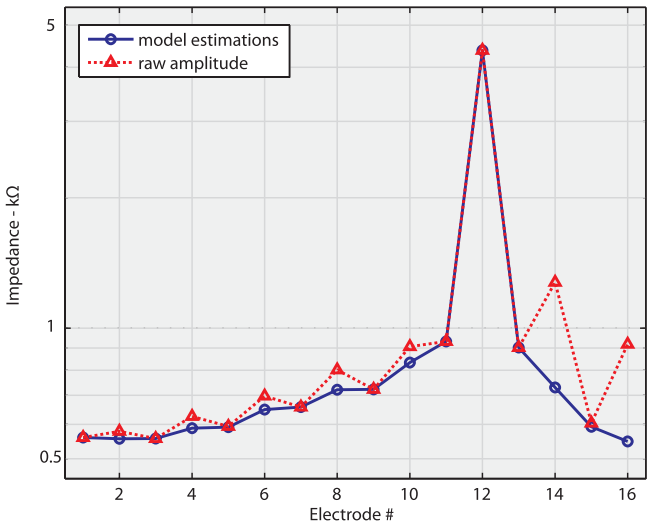

Figure 13. Transimpedance recording made with S7. Dotted lines: all transimpedance were estimated by measuring the peak-to-peak amplitude, solid line: model-based estimations.

For that matter, the influence of electrical stimulation on contact impedance is also discussed in the next section.

Our recordings revealed different levels of distortion (see figure 12, panel (C)) which could be related to different levels of polarization. Neglecting this phenomenon could provide an erroneous estimation of the transimpedance matrix and thus impair the efficiency of the PA strategy. Triangles in figure 13 illustrate the transimpedance pattern obtained by measuring the peak-to-peak amplitude of the recordings. This pattern shows oscillations between high and low values for even and odd electrodes, respectively. It is likely that this pattern does not have any physical basis and only results from measurement artifacts. To obtain a more relevant estimation of the transimpedance a simple electrical model derived from the one used for contact impedances was used to estimate the resistive part of the impedance. This model consisted of a CPE in series with a resistive load representing the actual transimpedance. As for the contact impedance model, the influence of C_p was included in the current input waveform. The circles in figure 13 illustrate the smoother transimpedance pattern obtained using this alternative model.

Table 4. Percentage of variation of model parameters estimations at 25 μA and 100 μA relative to the estimations made at 50 μA amplitude stimuli. Analysis based on the recordings made with all subjects on a subset of five electrodes (E1, 4, 8, 12 and 16)

% var.	100 μA	25 μA
Ra	−0.1 (±1.5)	−6.3 (±1.1)
Y_0	30.9 (±11.7)	32.5 (±13.2)
α	−2.2 (±1.2)	−1.5 (±1.3)

The different profiles reported for S7 and S8 are very specific and we expected them to be isolated cases. However, it remains complicated to evaluate on which time scale the deactivation or activation of an electrode may induce important changes in its electro-chemical behavior and its active area and whether these changes are reversible or not.

We assume that the observed distortion results from a partial electrode polarization based on our observations. Hence, with this model we isolate the contribution of the surface polarization and focus on the resistive part of the impedance to obtain a more relevant estimation of the transimpedance. However, the fact that the physical phenomenon is still not clearly identified prevents us from a clear interpretation of the polarization parameters of the present model. Further investigation is thus needed to better understand the ongoing phenomenon and verify our hypothesis.

5.2. *Experiment 2: Contact impedance model*

The electrical model presented here provides a good description of all contact impedance waveforms recorded both *in vitro* and in CI users. Importantly, it also provides a better fit to the measurements than the usual RC model used in previous impedance studies with CI listeners (Vanpoucke *et al* 2004a, Tykocinski *et al* 2005).

5.2.1. Sensitivity of model parameters. Multiple conditions were tested to evaluate the robustness of model parameters. This enabled us to confirm the stability of the estimated access resistance which was the main objective of the present study. However, it also highlighted the larger sensitivity of other model parameters (Y_0 and α, figure 10).

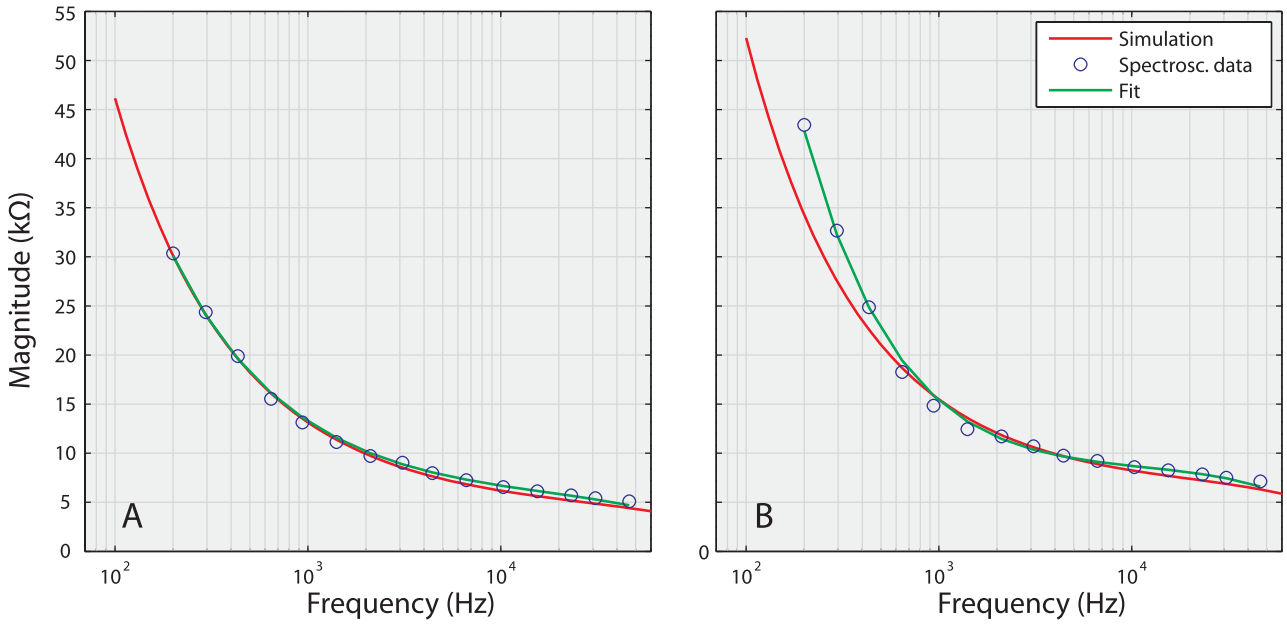

Figure 14. Examples of magnitude spectra of contact impedance for subject S7, panel A and subject S1, panel (B) The circles indicate the spectroscopy data points, the green curves represent the output of the contact impedance model applied on the spectroscopy data and the red curves represent the simulated spectrum based on the model estimations obtained using biphasic pulses.

Schwan and Maczuk (1965) first reported the variability of polarization parameters (electrode-fluid interface only) at low frequency when varying the current density. Later, Geddes (1997) extended this finding by demonstrating that for current densities increasing from 0.01 to 1 mA cm^{-2} (for platinum electrodes and considering resistor-capacitor models), the polarization resistance and capacitance exhibit a monotonic decrease and increase respectively. Beyond this value, both polarization parameters dramatically vary as a function of the current density. While here, all recordings were carried out at a moderate level, the current density exceeded the limit reported by Schwan and Maczuk (1965) (25 mA cm^{-2} for 50 μA). The variability of polarization parameters observed here may thus be explained by a strongly nonlinear electrochemical behavior. In the opposite, the access resistance represents the equivalent resistance of the electrical path between the electrode's surface and the ground electrode. As a consequence we would not excpect R_a to vary with stimulation level. To address this question, we report in table 4 the variation of model parameters estimations (and the standard error) made on a subset of five electrodes at 25 μA and 100 μA compared to the reference condition at 50 μA. It can be observed that the influence of stimulation level is moderate on the access resitance while it has a much larger effect on Y_0 which is consistent with previous observations. However, it is important to note that Y_0 and α are interdependent, by definition of the equation 1, so that a variation of both Y_0 and α in oppostite directions has less influence on the waveform than the variation of only one of them.

We also noted a divergence in the estimations of Y_0 when using biphasic pulses or impedance spectroscopy (figure 10(B)). These differences observed between biphasic pulses and sine wave stimuli might be partly explained by a difference in the stimulation level but also by differences in their spectral content. Geddes (1997) reported that the variability of polarization parameters is larger at low frequency. Compared to the range of frequencies used for spectroscopy, the frequency content of the biphasic pulse waveform is limited in the low frequency region by the phase duration value and in the high frequency region by the product $Ra \times Cp$. Figure 14 displays the magnitude spectrum of contact impedance recorded in two CI subjects (circles, S7 left panel, and S1 right panel). Green curves indicate the output of the contact impedance model applied on these data. Red curves represent the simulated magnitude spectrum based on the model parameters estimation using biphasic pulses. One can see on the right panel that, as expected, the spectral and temporal model estimations are very consistent between 600 Hz and 10 kHz. However, below and beyond this range, the spectral and temporal estimations diverge. On the left panel, both estimations were surprisingly consistent over the entire frequency range. These observations demonstrate that impedance spectroscopy can provide more information than biphasic pulses and thus represent a relevant way of estimating the contact impedance. Unfortunately, the protocol used here would require further optimization to reduce the duration of the measurement (approximately 25 min for 16 electrodes) for a clinical use.

5.2.2. Evolution of impedances over time. In the perspective of using impedance estimations for multipolar strategies one also has to consider the stability of impedances over time.

As mentioned before, Duan *et al* (2004) pointed out that contact impedances are strongly dependent on the coupling between the electrode surface and the cochlear medium. The presence of different biological materials with different electrical properties may influence impedances. It is thus important to consider the evolution of this coupling over time and on different time scales.

It is known that impedances first dramatically increase post-implantation because of a combination of electrodechemical

Table 5. Variation of model parameters (%) for electrodes 1, 8, 16 recorded with S2 and S6. Recordings were made with a delay of five months for S2 and three months for S6.

	Electrode	ΔRa	ΔY_0	$\Delta\alpha$
S2 ($\Delta t = 5$ months)	1	−2.4	−19.9	+4.4
	8	−6.9	−18.8	+4.0
	16	+4.0	+38.6	+8.8
S6 ($\Delta t = 3$ months)	1	−0.6	−8.8	+1.4
	8	+1.1	−8.1	+2.5
	16	−2.6	−29.8	+7.9

and biological immune reactions. The activation of the device, and electrical stimulation itself, is also thought to induce additional electrochemical and biological reactions, yielding a fast decrease of impedances (Duan *et al* 2004, Newbold *et al* 2004, Leone *et al* 2017). While a comparable stabilization process is thought to occur with all CI users, the amplitude of the impedance changes may vary, from one patient to another, with the post-operation time as well as patients' physiological reaction to the surgery (e.g. swelling, infection, healing time). It may thus account for an important part of the *inter*-subject variability in impedances.

Wilk *et al* (2016) and Leone *et al* (2017) showed that after one month post-activation, impedances remain relatively stable for most patients. Here, all patients were tested several years after cochlear implantation. Clinical history confirmed that their impedance had been stable for several months or years. To assess possible impedance changes on a short time scale, impedances were estimated with the clinical software at the beginning and at the end of the session. Overall, the 128 electrodes tested exhibited an average variation of 1.2% across a session. Additional contact impedance data were recorded on a subset of electrodes with S2 and S6, respectively, five months and three months after the initial session. Table 5, reports the percentage of variation of the model parameters relative to the initial session. A delay of several months yielded a moderate variation for both R_a and α and, again, a slightly larger variation for Y_0.

Nevertheless, it seems important to update these estimations on a regular basis to monitor the evolution of the device.

Impedances may also be related to specific factors such as the anatomical features, the electrode position and the insertion depth. For example the facial nerve canal, close to the first turn of the cochlea (Vanpoucke *et al* 2004b, Erixon *et al* 2008), is thought to provide a possible current pathway. Electrodes located close to the facial nerve canal would thus have low impedances (Vanpoucke *et al* 2004b, Duan *et al* 2004, Micco and Richter 2006). In the opposite the proximity of the cochlear acqueduct is thought to induce an important growth of fibrous tissue and thus an increase of impedance.

Majdi *et al* (2015), in retinal prostheses and Giardina *et al* (2017), in the CI field, demonstrated *in vitro* that impedances may provide information about the electrode position and the proximity of various anatomical elements (e.g. neural tissues, bone, etc). Here, electrode-to-modiolus distances could be estimated from CT images in five of our patients but no significant relationship could be identified between the electrodes impedance and the distance to the modiolus. While electrode displacement remains a rare complication (Mittmann *et al* 2015, Dietz *et al* 2016), we can wonder whether micro-movements of the electrode array due to fibrosis or ossification may yield significant impedance changes.

5.3. Implications for future multipolar strategies in cochlear implants and other neural prostheses

The results of these different experiments may have direct implications for the implementation of the PA strategy.

First, we have validated the necessary assumption of resistivity on which the PA strategy relies. We also observed that the summation of different electrical fields generated by biphasic pulses is a linear process which can result in transient artifacts. While the influence of these artifacts at the perceptual level seems difficult to predict, it results in potentially high-amplitude voltage peaks in regions where we would expect to cancel the overall electrical field. Here we proposed using single-cycle sine waves as an alternative to square pulses to prevent from generating uncontrolled voltage peaks in the inner ear.

Second, we have seen that the estimation of the transimpedance matrix, which is the key element for the implementation of the PA strategy, is relatively stable over time (data not shown here) and when varying the stimulation level (ranging from 25 to 100 μA). However, transimpedances can be dramatically affected by the partial polarization of inactive electrodes. While this distortion does not occur in all patients and all electrodes, when needed, a simple electrical model can be used to estimate the transimpedances.

Third, a slightly more complex model including a CPE was proposed to estimate the diagonal terms of the impedance matrix. We demonstrated that this model could fit our data in the temporal and spectral domains (spectroscopy) and provided better estimates than RC models used in the past.

As discussed along this article, the present findings may have implications in the design of future multi-electrode strategies for CIs. However, their direct application is certainly not restricted to the CI field. Comparable issues may be found in other auditory prostheses such as auditory brainstem implant and auditory midbrain implant but also in the field of visual prostheses or even deep brain stimulation (Slama 2015, Shepherd 2016, Spencer *et al* 2016). Recently, Spencer *et al* (2016) extended the principle of multi-electrode focused stimulation to two-dimensional electrode arrays in retinal prostheses. While the application of such a technique is even more challenging in two-dimensional arrays, their results are promising and motivate future research in this direction.

All neural implants based on direct stimulation involve active metallic electrodes in contact with biological tissues and/or fluids. As a result, they are all necessarily confronted to electrodes polarization issues. Besides, the recent aforementioned auditory and visual prostheses consist of closely packed arrays of micro-electrodes (e.g. up to 1500 in retinal implant clinical trials, Wilke *et al* (2011)). In such conditions, understanding the electrochemical properties of the implanted electrodes (e.g. polarization, passivation) as well as improving

spatial selectivity by means of advanced multi-electrode stimulation strategies remain important challenges (Horsager *et al* 2010, Weiland and Humayun 2014).

Acknowledgments

The authors sincerely thank Paddy Boyle, Leo Litvak, Yves Cazals, and the CHU of Montpellier for their help, CI subjects for their participation and two anonymous reviewers for their helpful comments on an earlier version of this article. This work was supported by the Agence Nationale de la Recherche (France), Grant No. ANR-11-PDOC-0022.

Appendix. Implementation of the polarization impedance model

A.1. Contact impedance model equations

A.1.1. Complete model. The polarization impedance was modeled using the equivalent electrical circuit of figure 7. As mentionned in section 5.2.1, electrical recordings using the experimental load board suggest that the current waveform delivered by an electrode is affected by the presence of the parasitic capacitance, C_p. As a result, in the present model, we considered a biphasic current pulse with exponential transients (time constant τ, defined as $R_a \times C_p$) as the input signal. If we consider the input current waveform in figure A1, its mathematical expression can be written as in equation (A.1), where $H(t)$ is the Heaviside step function.

To be able to compute an analytical solution, this problem is converted in the Laplace domain, yielding equation (A.2).

$$I(t) = I_0 \cdot \left[(1 - \mathrm{e}^{-\frac{t}{\tau}}) - 2 \cdot (1 - \mathrm{e}^{-\frac{(t-T_p)}{\tau}}) \cdot H(T_p) + (1 - \mathrm{e}^{-\frac{(t-2\cdot T_p)}{\tau}}) \cdot H(2 \cdot T_p) \right] \quad \text{(A.1)}$$

$$\mathscr{L}(I(t)) = I_0 \cdot \left[(\frac{1}{s} - \frac{1}{s+\frac{1}{\tau}}) - 2 \cdot \mathrm{e}^{-T_p \cdot s} (\frac{1}{s} - \frac{1}{s+\frac{1}{\tau}}) + \mathrm{e}^{-2 \cdot T_p \cdot s} (\frac{1}{s} - \frac{1}{s+\frac{1}{\tau}}) \right] \quad \text{(A.2)}$$

$$Z(s) = R_a + \frac{1}{C_b \cdot s} + \frac{1}{Y_0} \cdot \left(\frac{1}{s^\alpha + \frac{1}{R_f \cdot Y_0}} \right). \quad \text{(A.3)}$$

The voltage across the entire circuit in the Laplace domain (equation (A.4)) is obtained by multiplying equation (A.2) and the overall circuit impedance (without C_p) whose Laplace transform is given by equation (A.3).

$$U(s) = I_0 \cdot \left[Z(s) \cdot \frac{1}{s} - 2 \cdot \mathrm{e}^{-Tp \cdot s} \cdot Z(s) \cdot \frac{1}{s} + \mathrm{e}^{-2Tp \cdot s} \cdot Z(s) \cdot \frac{1}{s} \right] ... \\ ... - I_0 \cdot \left[Z(s) \cdot \frac{1}{s + 1/\tau} - 2 \cdot \mathrm{e}^{-Tp \cdot s} \cdot Z(s) \cdot \frac{1}{s + 1/\tau} + \mathrm{e}^{-2Tp \cdot s} \cdot Z(s) \cdot \frac{1}{s + 1/\tau} \right]. \quad \text{(A.4)}$$

After transformation back in the time domain, one can distinguish in this solution the contribution of a perfect square pulse and the contribution of the transients. The exact solution in the time domain can thus be written as in equations (A.5).

$$\begin{cases} U(t) = I_0 \cdot \left[f(t) \cdot H(0) - 2 \cdot f(t) \cdot H(T_p) + f(t) \cdot H(2 \cdot T_p) \right] ... \\ ... - I_0 \cdot \left[\tilde{f}(t) \cdot H(0) - 2 \cdot \tilde{f}(t) \cdot H(T_p) + \tilde{f}(t) \cdot H(2 \cdot T_p) \right] \\ \text{with,} \\ f(t) = \mathscr{L}^{-1}(Z(s) \cdot \frac{1}{s}) \\ \tilde{f}(t) = \mathscr{L}^{-1}(Z(s) \cdot \frac{1}{s+\frac{1}{\tau}}) \end{cases} . \quad \text{(A.5)}$$

To obtain an analytical solution, one needs to solve both $f(t)$ and $\tilde{f}(t)$. Let us start with $f(t)$ whose expression can be developed as in equations (A.6).

$$\begin{cases} f(t) = \mathscr{L}^{-1} \left(R_a \cdot \frac{1}{s} + \frac{1}{C_b \cdot s^2} + \frac{1}{Y_0 \cdot s} \cdot \frac{1}{s^\alpha + \frac{1}{R_f \cdot Y_0}} \right) \\ f(t) = R_a + \frac{t}{C_b} + g(t) \\ \text{with,} \\ g(t) = \mathscr{L}^{-1} \left(\frac{1}{Y_0 \cdot s} \cdot \frac{1}{s^\alpha + \frac{1}{R_f \cdot Y_0}} \right) \end{cases} . \quad \text{(A.6)}$$

$g(t)$ can then be expressed involving a geometric series (equation (A.7)).

$$\begin{cases} g(t) = \mathscr{L}^{-1} \left(\frac{1}{Y_0 \cdot s} \cdot \frac{1}{s^\alpha + \frac{1}{R_f \cdot Y_0}} \right) \\ g(t) = \frac{1}{Y_0} \cdot \mathscr{L}^{-1} \left(\frac{1}{s^{\alpha+1}} \cdot \sum_{k=0}^{\infty} \left(\frac{-1}{R_f \cdot Y_0 \cdot s^\alpha} \right)^n \right) \\ g(t) = \frac{1}{Y_0} \cdot \mathscr{L}^{-1} \left(\frac{1}{s^{\alpha+1}} \cdot \sum_{k=0}^{\infty} \left(\frac{-1}{R_f \cdot Y_0} \right)^n \cdot \frac{1}{s^{\alpha n}} \right) \\ g(t) = \frac{1}{Y_0} \cdot \mathscr{L}^{-1} \left(\sum_{k=0}^{\infty} \left(\frac{-1}{R_f \cdot Y_0} \right)^n \cdot \frac{1}{s^{\alpha n + \alpha + 1}} \right) \end{cases} . \quad \text{(A.7)}$$

At this stage, to be able to solve this expression, one needs to involve the Γ function as in equations (A.8) which introduces a known Laplace function, $\Gamma(x)/s^x$.

$$g(t) = \frac{1}{Y_0} \cdot \sum_{k=0}^{\infty} \left(\frac{-1}{R_f \cdot Y_0} \right)^n \cdot \mathscr{L}^{-1} \left(\frac{\Gamma(\alpha n + \alpha + 1)}{s^{\alpha n + \alpha + 1}} \cdot \frac{1}{\Gamma(\alpha n + \alpha + 1)} \right). \quad \text{(A.8)}$$

We can then write:

$$\begin{cases} g(t) = \frac{1}{Y_0} \cdot \sum_{k=0}^{\infty} \left(\frac{-1}{R_f \cdot Y_0} \right)^n \cdot t^{\alpha n + \alpha} \cdot \frac{1}{\Gamma(\alpha n + \alpha + 1)} \\ g(t) = \frac{1}{Y_0} \cdot \sum_{k=0}^{\infty} \left(\frac{-1}{R_f \cdot Y_0} \right)^n \cdot \frac{t^{\alpha n}}{\Gamma(\alpha n + \alpha + 1)} \cdot t^\alpha \end{cases} . \quad \text{(A.9)}$$

A final analytical solution can be written using the Mittag–Leffler function (Podlubny and Kacenak 2012), whose general expression is given by the equation (A.10) and by including the expression of $f(t)$ in the equation (A.5).

$$E_{\gamma,\beta}(t) = \sum_{k=0}^{\infty} \frac{t^k}{\Gamma(\gamma \cdot k + \beta)} \quad \text{(A.10)}$$

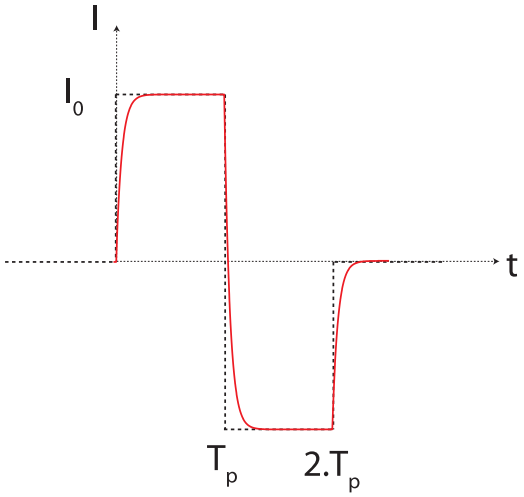

Figure A1. Illustration of the input current waveform. I_0 is the current amplitude and T_p is the phase duration.

$$g(t) = \frac{t^{\alpha}}{Y_0} \cdot E_{\alpha,\alpha+1}\left(\frac{-t^{\alpha}}{R_f \cdot Y_0}\right). \tag{A.11}$$

Following the same procedure one can solve $\tilde{f}(t)$.

$$\begin{cases} \tilde{f}(t) = \mathscr{L}^{-1}\left(R_a \cdot \frac{1}{s+1/\tau} + \frac{1}{C_b \cdot s} \cdot \frac{1}{s+1/\tau} + \frac{1}{Y_0} \cdot \frac{1}{s^{\alpha}+\frac{1}{R_f \cdot Y_0}} \cdot \frac{1}{s+1/\tau}\right) \\ \tilde{f}(t) = R_a \cdot \mathrm{e}^{-\frac{1}{\tau}} + \frac{\tau}{C_b} \cdot (1-\mathrm{e}^{-\frac{t}{\tau}}) + \frac{1}{Y_0} \cdot (\tilde{g}(t) * \mathrm{e}^{-\frac{t}{\tau}}) \\ \tilde{g}(t) = \mathscr{L}^{-1}\left(\frac{1}{s^{\alpha}+\frac{1}{R_f \cdot Y_0}}\right) \end{cases} \tag{A.12}$$

$$\tilde{g}(t) = t^{\alpha-1} \cdot E_{\alpha,\alpha}\left(\frac{-t^{\alpha}}{R_f \cdot Y_0}\right). \tag{A.13}$$

A.1.2. Simplification. In this study the parameter R_f was removed from the model. In this case the overall solution can be simplified by replacing $f(t)$ and $\tilde{f}(t)$ in equation (A.5) by $f_{simplified}(t)$ and $\tilde{f}_{simplified}(t)$ as in equation (A.14).

$$\begin{cases} f_{simplified}(t) = R_a + \frac{t}{C_b} + \frac{1}{Y_0 \cdot \Gamma(\alpha+1)} \cdot t^{\alpha} \\ \tilde{f}_{simplified}(t) = R_a \cdot \mathrm{e}^{-\frac{1}{\tau}} + \frac{\tau}{C_b} \cdot (1-\mathrm{e}^{-\frac{t}{\tau}}) + \frac{1}{Y_0} \cdot t^{\alpha} \cdot E_{1,\alpha+1}\left(\frac{-t}{\tau}\right) \end{cases}. \tag{A.14}$$

AQ8 ## ORCID iDs

Quentin Mesnildrey https://orcid.org/0000-0003-2149-3599

AQ9 ## References

AQ10
Abbas P and Miller C 2006 Biophysics and physiology *Cochlear*
AQ11 *Implant. Audit. Prosthese Electr. Hear.* shar edn (Berlin: Springer) ch 5, pp 149–212
AQ12 Barbour B 2014 Electronics for electrophysiologists
Baumann S, Wozny D, Kelly S and Meno F 1997 The electrical conductivity of human cerebrospinal fluid at body temperature *IEEE Trans. Biomed. Eng.* **44** 220–5
Bondarenko A and Ragoisha G 2005 EIS spectrum analyser *Prog. Chemom. Res.* ed A L Pomerantsev (New York: Nova Science Publishers) pp 89–102
Brendel M, Rottmann T, Lenarz T and Buechner A 2013 Performance of the Harmony TM behind-the-ear processor with the first generation of advanced bionics TM implant systems *Cochlear Implants Int.* **14** 36–44
Burdon R 2008 Short note: coefficients of variation in variables with bounded scales *Silvae Genet.* **57** 179–80
Chatterjee M and Kulkarni A 2014 Sensitivity to pulse phase duration in cochlear implant listeners: effects of stimulation mode *J. Acoust. Soc. Am.* **136** 829–40
Clopton B and Spelman F 1982 Neural mechanisms relevant to the design of an auditory prothesis. Location and electrical characteristics
Desmadryl G, Gaboyard-Niay S, Brugeaud A, Travo C, Broussy A, Saleur A, Dyhrfjeld-Johnsen J, Wersinger E and Chabbert C 2012 Histamine H 4 receptor antagonists as potent modulators of mammalian vestibular primary neuron excitability *Br. J. Pharmacol.* **167** 905–16
Dietz A, Wennström M, Lehtimäki A, Löppönen H and Valtonen H 2016 Electrode migration after cochlear implant surgery: more common than expected? *Eur. Arch. Oto-Rhino-Laryngol.* **273** 1411–8
Duan Y, Clark G and Cowan R 2004 A study of intra-cochlear electrodes and tissue interface by electrochemical impedance methods *in vivo Biomaterials* **25** 3813–28
Dymond A 1976 Characteristics of the metal-tissue interface of stimulation electrodes *IEEE Trans. Biomed. Eng.* **23** 274–80
Erixon E, Hogstorp H, Wadin K and Rask-andersen H 2008 Variational anatomy of the human cochlea: implications for cochlear implantation *Otol. Neurotol.* **30** 14–22
Finley C, Wilson B and White M 1990 Models of neural responsiveness to electrical stimulation *Cochlear Implants* (*Models of the Electrically Stimulated Ear*) (New York: Springer) ch 5, pp 55–96
Franks W, Schenker I, Schmutz P and Hierlemann A 2005 Impedance characterization and modeling of electrodes for biomedical applications *IEEE Trans. Biomed. Eng.* **52** 1295–302
Fridman G and Karunasiri R 2010 Removing artifact in evoked compound action potential recordings in neural stimulators
Friesen L, Shannon R, Baskent D and Wang X 2001 Speech recognition in noise as a function of the number of spectral channels: comparison of acoustic hearing and cochlear implants *J. Acoust. Soc. Am.* **110** 1150
Frijns J, Dekker D and Briaire J 2011 Neural excitation patterns induced by phased-array stimulation in the implanted human cochlea *Acta Otolaryngol.* **131** 362–70
Geddes L A 1997 Historical evolution of circuit models for the electrode-electrolyte interface *Ann. Biomed. Eng.* **25** 1–14
George S, Wise A, Shivdasani M, Shepherd R and Fallon J 2014 Evaluation of focused multipolar stimulation for cochlear implants in acutely deafened cats *J. Neural Eng.* **11** 065003
Giardina C, Krause E, Koka K and Fitzpatrick D 2017 Impedance measures during *in vitro* cochlear implantation predict array positioning *IEEE Trans. Biomed. Eng.* **65** 327–35
Gouy M 1910 Sur la constitution de la charge électrique à la surface d' un électrolyte *J. Phys. Théor. Appl.* **9** 457–68
Grahame D 1947 The electrical double-layer and the theory of electrocapillarity *Chem. Rev.* **41** 441–501
Grill W and Mortimer J 1994 Electrical properties of implant encapsulation tissue *Ann. Biomed. Eng.* **22** 23–33
Grimnes S and Martinsen O 2008 *Bioimpedance and Bioelectricity Basics* vol 2m 2nd edn (Oxford: Oxford University Press)
Horsager A, Greenberg R and Fine I 2010 Spatiotemporal interactions in retinal prosthesis subjects *Investig. Ophthalmol. Vis. Sci.* **51** 1223–33
Ifukube T and White R 1987 Current distributions produced inside and outside the cochlea from a scala tympani electrode array *IEEE Trans. Biomed. Eng.* **BME-34** 883–90

Kalkman R, Briaire J and Frijns J 2015 Current focussing in cochlear implants : An analysis of neural recruitment in a computational model *Hear. Res.* **322** 89–98

Kovacs G 1994 Introduction to the theory, design, and modeling of thin-film microelectrodes for neural interfaces *Enabling Technologies Cult Neural Networks* ed D A Stenger and T M McKenna, londo edn pp 121–65

Lario-García J and Pallàs-Areny R 2006 Constant-phase element identification in conductivity sensors using a single square wave *Sensors Actuators* A **132** 122–8

Leone C, Mosca F and Grassia R 2017 Temporal changes in impedance of implanted adults for various cochlear segments *Acta Otorhinolaryngol. Ital.* **37** 312–9

Litvak L M 2003 BEDCS bionic ear data collection system. Version 1.16, user manual *Technical Report* Advanced Bionics

López D, Durán A and Ceré S 2008 Electrochemical characterization of AISI 316L stainless steel in contact with simulated body fluid under infection conditions *J. Mater. Sci. Mater. Med.* **19** 2137–44

Majdi J, Minnikanti S, Peixoto N, Agrawal A and Cohen E 2015 Access resistance of stimulation electrodes as a function of electrode proximity to the retina *J. Neural Eng.* **12** 016006

Marozeau J, McDermott H, Swanson B and McKay C 2015 Perceptual interactions between electrodes using focused and monopolar cochlear stimulation *J. Assoc. Res. Otolaryngol.* (https://doi.org/10.1007/s10162-015-0511-2)

McDermott H 2004 Music perception with cochlear implants: a review *Trends Amplif.* **8** 49–82

Mesnildrey Q and Macherey O 2015 Simulating the dual-peak excitation pattern produced by bipolar stimulation of a cochlear implant: effects on speech intelligibility *Hear. Res.* **319** 32–47

Micco A and Richter C 2006 Tissue resistivities determine the current flow in the cochlea *Curr. Opin. Otolaryngol. Head Neck Surg.* **14** 352–5

Miller A, Smith D and Pfingst B 1999 Across-species comparisons of psychophysical detection thresholds for electrical stimulation of the cochlea: II. Strength-duration functions for single, biphasic pulses *Hear. Res.* **135** 47–55

Mittmann P, Rademacher G, Mutze S, Ernst A and Todt I 2015 Electrode migration in patients with perimodiolar cochlear implant electrodes *Audiol. Neurotol.* **20** 349–53

Moon A, Zwolan T and Pfingst B 1993 Effects of phase duration on detection of electrical stimulation of the human cochlea *Hear. Res.* **67** 166–78

Nelder J and Mead R 1965 A simplex method for function minimization *Comput. J.* **7** 308–13

Newbold C, Richardson R, Huang C, Milojevic D, Cowan R and Shepherd R 2004 An *in vitro* model for investigating impedance changes with cell growth and electrical stimulation: implications for cochlear implants *J. Neural Eng.* **1** 218–27

Pfingst B 1988 Comparisons of psychophysical and neurophysiological studies of cochlear implants *Hear. Res.* **34** 243–51

Pham P, Roux S, Matonti F, Dupont F, Agache V and Chavane F 2013 Post-implantation impedance spectroscopy of subretinal micro-electrode arrays, OCT imaging and numerical simulation: towards a more precise neuroprosthesis monitoring tool *J. Neural Eng.* **10** (https://doi.org/10.1088/1741-2560/10/4/046002)

Podlubny I and Kacenak M 2012 MLF—Mittag–Leffler function

Scholvin J, Kinney J, Bernstein J, Moore-Kochlacs C, Kopell N, Kopell N, Fonstad C and Boyden E 2016 Close-packed silicon microelectrodes for scalable spatially oversampled neural Recording *IEEE Trans. Biomed. Eng.* **63** 120–30

Schwan H and Calvin F 1957 Capacitive properties of body tissues *Circ. Res.* **5** 439–43

Schwan H and Maczuk J 1965 Electrode polarization impedance: limits of linearity *Proc. 18th ACEMB* vol 5 (Philadelphia)

Shepherd R 2016 *Neurobionics: the Biomedical Engineering of Neural Prostheses* (New York: Wiley)

Slama M 2015 Toward new generation auditory brainstem implants: electrical and optogenetic stimulation of the cochlear nucleus (https://dash.harvard.edu/handle/1/17295889)

Smith Z, Parkinson W and Long C 2013 Multipolar current focusing increases spectral resolution in cochlear implants *Annual Int. Conf. of IEEE Engineering in Medicine and Biology Society* pp 2796–9

Spencer T, Fallon J, Thien P and Shivdasani M 2016 Spatial restriction of neural activation using focused multipolar stimulation with a retinal prosthesis *Investigative Ophthalmol. Vis. Sci.* **57** 3181–91

Stickney G, Loizou P, Mishra L, Assmann P, Shannon R and Opie J 2006 Effects of electrode design and configuration on channel interactions *Hear. Res.* **211** 33–45

Strelioff D 1973 A computer simulation of the generation and distribution of cochlear potentials *J. Acoust. Soc. Am.* **54** 620–9

Suesserman M and Spelman F 1993 Quantitative *in vivo* measurements of inner ear tissue resistivities: I. *In vitro* characterization *IEEE Trans. Biomed. Eng.* **40** 1032

Suesserman M, Spelman F and Rubinstein J 1991 *In vitro* measurement and characterization of current density profiles produced by nonrecessed, simple recessed, and radially varying recessed stimulating electrodes *IEEE Trans. Biomed. Eng.* **38** 401–8

Tognola G, Pesatori A, Norgia M, Parazzini M, Di Rienzo L, Ravazzani P, Burdo S, Grandori F and Svelto C 2007 Numerical modelling and experimental measurements of the electric potential generated by cochlear implants in physiological tissues *IEEE Trans. Instrum. Meas.* **56** 187–1993

Topalov A, Cherevko S, Zeradjanin A, Meier J, Katsounaros I and Mayrhofer K 2014 Towards a comprehensive understanding of platinum dissolution in acidic media *Chem. Sci.* **5** 631–8

Townshend B and White R 1987 Reduction of electrical interaction in auditory prostheses *IEEE Trans. Biomed. Eng.* **11**

Tykocinski M, Cohen L and Cowan R 2005 Measurement and analysis of access resistance and polarization impedance in cochlear implant recipients *Otol. Neurotol.* **26** 948–56

van den Honert C and Kelsall D 2007 Focused intracochlear electric stimulation with phased array channels *J. Acoust. Soc. Am.* **121** 3703–16

Vanpoucke F, Zarowski A and Peeters S 2004a Identification of the impedance model of an implanted cochlear prosthesis from intracochlear potential measurements *IEEE Trans. Biomed. Eng.* **51** 2174–83

Vanpoucke F, Zarowski A, Casselman J, Frijns J and Peeters S 2004b The facial nerve canal: an important cochlear conduction path revealed by Clarion electrical field imaging *Otol. Neurotol.* **25** 282–9

von Compernolle D 1985 A computational model of the COchlea used with cochlear prothesis patients *IEEE Int. Conf. on Acoustics, Speech, and Signal Processing* pp 427–9

Weiland J and Humayun M 2014 Retinal prosthesis *IEEE Trans. Biomed. Eng.* **61** 1412–24

Wieckowski A 1999 *Interfacial Electrochemistry: Theory: Experiment, and Applications* (New York: Marcel Dekker)

Wilk M, Hessler R, Mugridge K, Jolly C, Fehr M, Lenarz T and Scheper V 2016 Impedance changes and fibrous tissue growth after cochlear implantation are correlated and can be reduced using a dexamethasone eluting electrode *PLoS One* **11** e0147552

Wilke R G, Moghadam G K, Lovell N H, Suaning G J and Dokos S 2011 Electric crosstalk impairs spatial resolution of multi-electrode arrays in retinal implants *J. Neural Eng.* **8** (https://doi.org/10.1088/1741-2560/8/4/046016)